JOURNAL OF MATERIALS SCIENCE 18 (1983) 2297–2304

Crystallization of the metallic glass $Fe_{80}B_{12}Si_8$

C. F. CHANG, J. MARTI
Corporate Research and Development, Allied Chemical Corporation, Morristown, New Jersey 07960, USA

Crystallization of the metallic glass $Fe_{80}B_{12}Si_8$ has been studied by differential scanning calorimetry, X-ray diffraction and transmission electron microscopy. Samples were annealed isothermally for 15 to 1400 min between 633 and 753 K. The crystalline phases observed are α(Fe, Si) and Fe_3B in sequence, with dendritic and cylindrical morphology, respectively. The distribution of α(Fe, Si) particles is rather uniform in the bulk but very non-uniform near both surfaces. The growth of these particles obeys a $t^{1/2}$ law and is diffusion controlled.

1. Introduction

Metallic glasses to be used in applications at high frequencies ($f \geqslant 50$ kHz) have recently been developed [1, 2]. The good high-frequency properties in these glasses have been shown to be the result of introduction of a small amount of crystallinity by suitable annealing [1, 2]. It has further been shown that both the volume fraction of crystallites and the nature of the precipitated crystalline phases are important [3]. To further the understanding of these observed features, a detailed knowledge of the crystallization behaviour and kinetics in these and other related glasses is necessary. In the Fe–B–Si system, we have found that the alloy $Fe_{80}B_{12}Si_8$, which is close in composition to a commercial high-frequency alloy, $Fe_{79}B_{16}Si_5$ (Metglas® 2605-S3) [2], exhibits two well-separated exothermic peaks upon heating, and hence, each phase can be studied independently. In the present investigation, attempts have been made (1) to identify the phases and morphologies in the alloy, (2) to study the nucleation and growth behaviour of each phase, and (3) to compare the crystallization behaviours observed at the surface and in the bulk of the sample.

2. Experimental procedure

The metallic glass $Fe_{80}B_{12}Si_8$ was prepared from constituent elements of at least 99.8% purity by planar flow casting [4] in vacuum. The crystallization behaviour of the as-cast sample was studied by differential scanning calorimetry (DSC). The reaction was recorded by a Perkin-Elmer DSC-2. The crystalline phases were identified using X-ray diffraction (XRD) with Cu$K\alpha$ radiation and by selected-area electron diffraction in a transmission electron microscope (TEM). The microstructures were studied by TEM. Samples were thinned for TEM by electropolishing in an electrolyte consisting of 20% perchloric acid in ethyl alcohol at 253 K. The foils were thinned in a twin jet Fischione electropolisher. For the areas near the surfaces, the side of interest was protected with a mask. The compositional profile across the thickness of the ribbon was studied by Auger electron spectroscopy (AES).

3. Results and discussion

3.1. Differential scanning calorimetry

Fig. 1 illustrates the DSC recording obtained for a heating rate of 2.5 K min^{-1}. There are two distinct crystallization exotherms separated by 40 K in temperature. While both peaks shift their positions with increasing heating rate the second peak grows with respect to the first peak. The shift of the peak temperature with heating rate was used to determine the activation energies of the reactions [5, 6]. The peak temperature, T_p, is related to the heating rate, ϕ, by

$$\ln\left(\frac{\phi}{T_p}\right) = C + \frac{E_a}{nRT_p} = C + \frac{E_c}{RT_p} \quad (1)$$

where C is a constant, E_a the apparent activation

0022–2461/83 $03.00 + .12

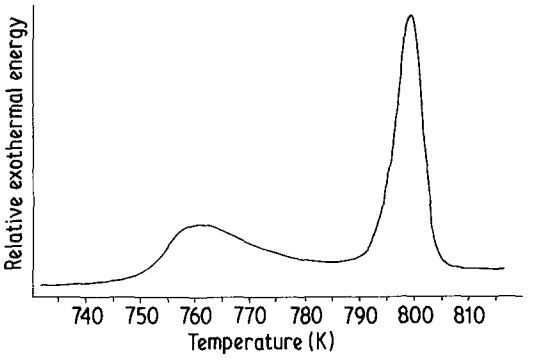

Figure 1 Differential scanning calorimeter recordings of the metallic glass alloy $Fe_{80}B_{12}Si_8$, obtained at a heating rate of 2.5 K min^{-1}.

energy, n the Avrami exponent, R the gas constant, and E_c the effective activation energy for crystallization. Fig. 2 shows the plot of $\ln(\phi/T_p)$ against $1/T_p$. The effective activation energies (E_c) determined from Fig. 2 are 3.7 (±0.2) eV and 3.6 (±0.2) eV for the first (lower T_p) and second (higher T_p) crystallized phase, respectively. The exponent n can be obtained from a fit to [5, 6]

$$\ln[-\ln(1-x)] = \text{const.} + n \ln t \quad (2)$$

where x is the crystalline fraction at time t, by assuming that the total heat evolved is proportional to x during the course of an isothermal anneal. Fig. 3 shows a plot of the integration of the DSC output $x(t)$ against isothermal annealing time t at 743 K. The linear relationship between $\ln\{-\ln[1-x(t)]\}$ and $\ln t$ shown in Fig. 4 indicates that the crystallization of the first phase obeys the Johnson–Mehl–Avrami equation [7]. The value n is determined as 2.8.

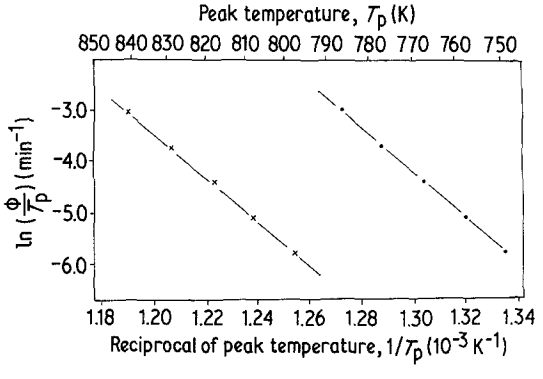

Figure 2 The plot of $\ln(\phi/T_p)$ against $1/T_p$ for determining the effective activation energy of the reaction. ϕ is the heating rate, T_p is the exotherm peak temperature.

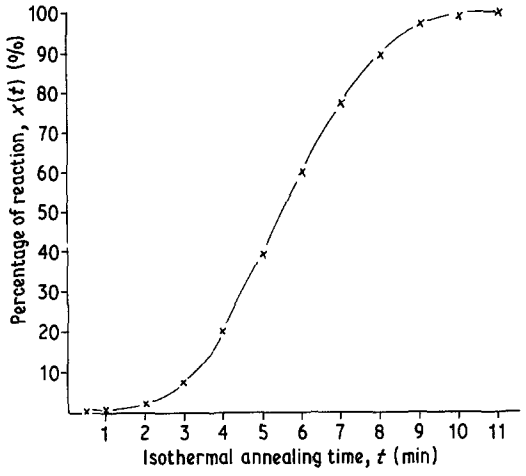

Figure 3 A plot of percentage of crystallization $x(t)$ against time t for $Fe_{80}B_{12}Si_8$ annealed at 743 K.

3.2. Structure, morphology of crystalline phase

The crystalline phases were identified by X-ray diffraction. The first crystallized phase is bcc

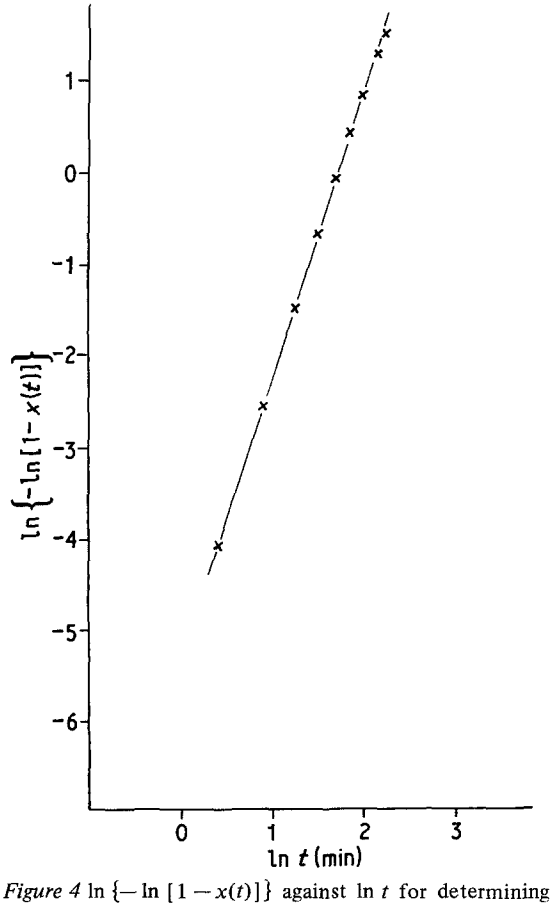

Figure 4 $\ln\{-\ln[1-x(t)]\}$ against $\ln t$ for determining the Avrami constant n for $Fe_{80}B_{12}Si_8$ annealed at 743 K.

Figure 5 Dendritic structure of α(Fe, Si) for $Fe_{80}B_{12}Si_8$ annealed at 693 K for 2 h.

α(Fe, Si) with $a_0 = 0.28636$ nm. The second crystallized phase is bc tetragonal Fe_3B with $a_0 = 0.863$ nm, $c_0 = 0.437$ nm. This is in agreement with other observations in Fe–B binary and Fe–B–Si ternary systems [6, 8]. When examined by TEM, the α(Fe, Si) phase shows the dendritic shape with two-, three-, four-fold symmetries, etc. (see Fig. 5). This kind of morphology is similar to that reported by Swartz *et al.* [8]. The dendritic growth direction of bcc crystals in isotropic environments is known to be along the cube axes. Thus, it is likely that the α(Fe, Si) microcrystal images are projections of one-, two- or three-dimensional ⟨001⟩ dendritic arms and branches. However, selected-area diffraction patterns for different morphologies are needed to confirm this point. Fig. 6 shows Fe_3B particles with cyclindrical morphology.

3.3. Nucleation and growth of α(Fe, Si) and Fe_3B

The time–temperature–transformation (T–T–T) curve for the onset of the nucleation of α(Fe, Si) on the surfaces of the ribbons was determined by X-ray diffraction (see Fig. 7). The α(Fe, Si) nucleates first on the shiny side (the surface away from the wheel) and then on the dull side (the surface on the wheel). It has been shown that the activation energy for nucleation (ΔH) is related to the incubation time (T) by the equation [9],

$$\frac{1}{\tau} = \frac{1}{\tau_0} \exp\left(-\frac{\Delta H}{RT}\right), \tag{3}$$

where τ_0 is the time constant, R is the gas constant and T is the annealing temperature. The activation energy for the nucleation at both surfaces of the α(Fe, Si) phase calculated from the slope of the plot of $\ln(1/\tau)$ against $1/T$ is 2.3 eV. The difference in the incubation time for nucleation between the two surfaces may indicate compositional/structural difference between the surface. The compositional depth profiles from both surfaces of the as-cast sample shows such variations in iron and boron. A layer depleted in iron and boron extends approximately 15 nm into the bulk from both sides (see Figs. 8 and 9). However, in a

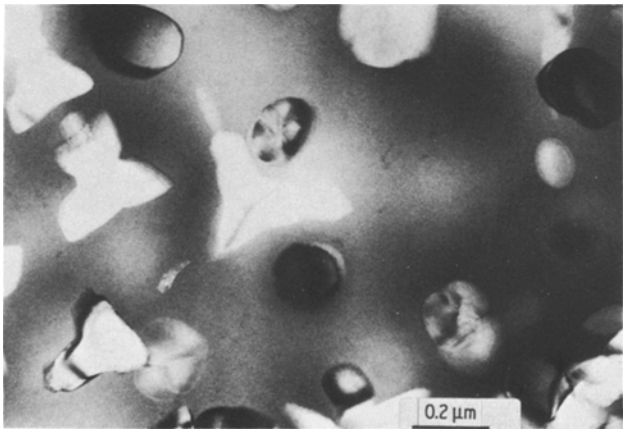

Figure 6 Cylindrical shape of Fe_3B for $Fe_{80}B_{12}Si_8$ annealed at 723 K for 2 h.

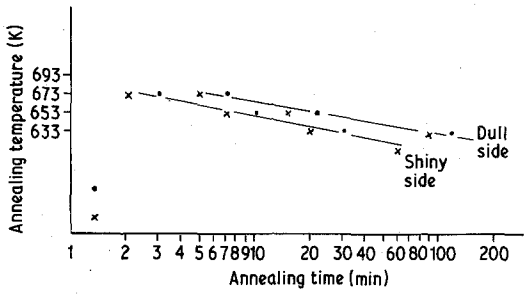

Figure 7 The time–temperature–transformation (T–T–T) curve for the onset of the nucleation of α(Fe, Si) on both surfaces of $Fe_{80}B_{12}Si_8$.

region between 15 and 30 nm below the surface little change of the composition of iron and boron is observed on the dull side. On the contrary, the shiny side shows the depletion of boron and the enrichment of iron. This compositional difference results in the earlier nucleation of α(Fe, Si) on the shiny side upon annealing owing to the increased driving force for this reaction. The present observation of shiny surface crystallization for vacuum-cast ribbon is contrary to that reported by Davis *et al.* on $Fe_{82}B_{12}Si_6$ alloy [10] (Metglas® 2605 S) which showed trace crystallinity on the dull side owing to the entrapment of air during casting under ambient conditions. TEM studies also show a significant microstructural difference between the two surfaces during crystallization of the present ribbon. For example, Figs. 10 and 11 show the microstructure of the sample annealed at 723 K for 30 min. Table I shows that the number of crystallites for α(Fe, Si) and Fe_3B phases is greater and their sizes are smaller on the dull side

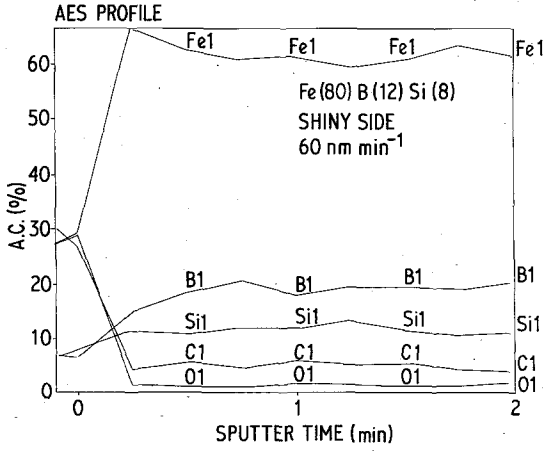

Figure 8 The compositional depth profiles of various elements in as-cast $Fe_{80}B_{12}Si_8$ obtained from the shiny side by Auger electron spectroscopy.

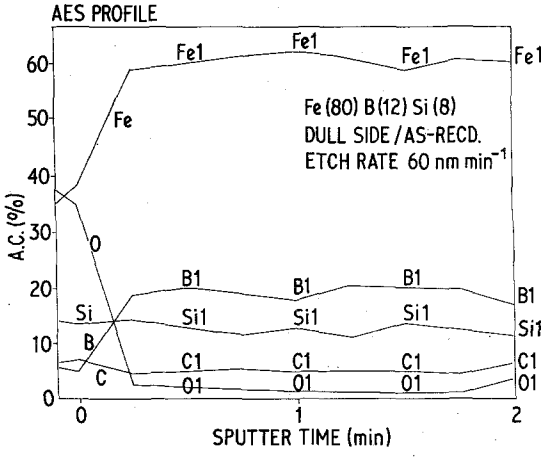

Figure 9 The compositional depth profiles of various elements in as-cast $Fe_{80}B_{12}Si_8$ obtained from the dull side by Auger electron spectroscopy.

than on the shiny side. No impingement of particles is observed at either surface, and thus the growth rate of α(Fe, Si) particles can be considered the same for both surfaces. Any size difference is then due to the difference in incubation time for nucleation.

TEM results show that the distribution of α(Fe, Si) particles is rather uniform in the bulk but very non-uniform on both surfaces. The kinetic study for the growth of the crystalline particles thus was concentrated on the bulk. Samples were annealed isothermally between 633 and 753 K for 15 to 1440 min and then examined by TEM. By assuming the largest particles to be the first nuclei to grow, the growth rates of the particles can be determined from the plot of size against annealing time. Figs. 12 and 13 show the maximum size of the particles (the dendritic arm lengths for α(Fe, Si) and the radii for Fe_3B) as a function of the square root of the annealing time. The linear relationship indicates that the growth process is diffusion controlled and follows the equation,

$$r = \alpha (Dt)^{1/2} \qquad (4)$$

where r is the size of the particles, α is a dimenionless parameter determined by the compositions near the particle matrix interface, D is the volume diffusion coefficient, and t is the annealing time. It is to be noted that in this alloy, although α(Fe, Si) particles nucleate first, they do not provide the nucleation site for Fe_3B. Both α(Fe, Si) and Fe_3B phases grow independently and follow the typical growth equation for primary nucleation [11].

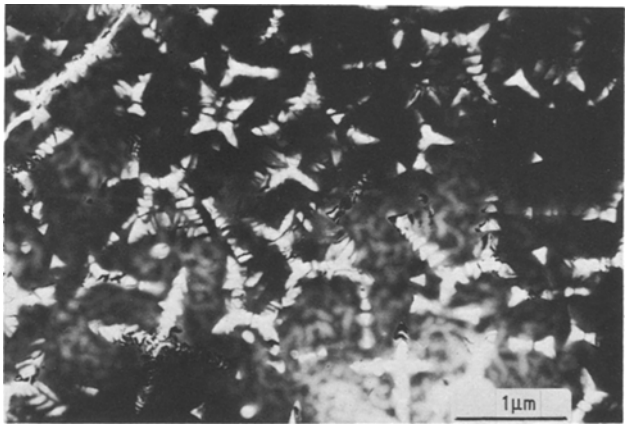

Figure 10 Microstructure of the shiny side for the $Fe_{80}B_{12}Si_8$ glass annealed at 723 K for 30 min.

By assuming α to be constant over the temperature range of the current investigation, Equation 4 can be rewritten as

$$\left[\frac{1}{\Delta t^{1/2}}(\Delta r)\right]^2 = \alpha^2 D = \alpha^2 D_0 \exp\left(-\frac{Q}{RT}\right) \quad (5)$$

where Q is the activation energy for the growth of particles. Q can then be determined from a plot of $\ln(\Delta r/\Delta t^{1/2})^2$ against $1/T$ as shown in Fig. 14. It is seen that massive nucleation is observed in the bulk for the sample annealed above 723 K. Particles tend to impinge upon each other and the growth rate is retarded significantly. Thus, the kinetic data above this temperature cannot reflect the true activation energy for the growth of the particles. We find from Fig. 14 that in this alloy the activation energy for the growth of α(Fe, Si) is about 1.6 eV, which is close to the value (1.8 eV) obtained by Koster and Herold for the growth of $\alpha Fe + Fe_3B$ eutectic spherulite in $Fe_{80}B_{20}$ (Metglas® 2605) [12]. It is to be noted that the solubility of B and Si in α-iron at 723 K is below 0.01 and 10 at%, respectively [13]. Thus, the nucleation and growth of α(Fe, Si) in amorphous $Fe_{80}B_{12}Si_8$ involve local rearrangement of Fe and Si and long range diffusion of B.

The incubation time (τ) for the nucleation of α(Fe, Si) in the bulk can be obtained by extrapolating the plot of size (r) against the time (t) down to $r = 0$ as shown in Fig. 13. With the incubation time τ thus obtained, the activation energy for the nucleation of α(Fe, Si) has been determined from a plot of $\ln(1/\tau)$ against $1/T$ (Fig. 14) as 2.3 eV. This value agrees with that (2.3 eV) for surface nucleation determined by X-ray diffraction (see above). This result indicates that the nucleation of α(Fe, Si) either in the bulk or on the surface is controlled by the same mechanism. The value of 2.3 eV for nucleation is also close to the value (2.1 eV) obtained by Koster and Herold [12].

3.4. Diffusion of boron in amorphous $Fe_{80}B_{12}Si_8$

As pointed out earlier, the growth of α(Fe, Si) is controlled by boron diffusion in the amorphous matrix. The kinetic data shown in Fig. 14 can be employed to estimate the diffusion coefficient of boron in $Fe_{80}B_{12}Si_8$ providing α is known. Because dendritic α(Fe, Si) grows along a particular direction, α can be estimated from Zener's equation for one-dimensional growth [14],

TABLE I The microstructural differences between the surface and the centre for the $Fe_{80}B_{12}Si_8$ alloy annealed at 723 K for 30 min

	Number of nucleation sites, $N_{\alpha\text{-Fe}}$ (10^6 mm^{-2})	Dendritic arm length (nm)	Volume fraction (α-Fe) (%)	Number of nucleation sites, N_{Fe_3B} (10^5 mm^{-2})	Radius of Fe_3B (nm)	Volume fraction (Fe_3B) (%)
Dull side (bottom surface)	5.3	890	21.3	2.4	80	0.3
Centre	1.9	830	21.6	2.8	70	0.8
Shiny side (top surface)	0.8	1250	28.4	1.6	200	5.9

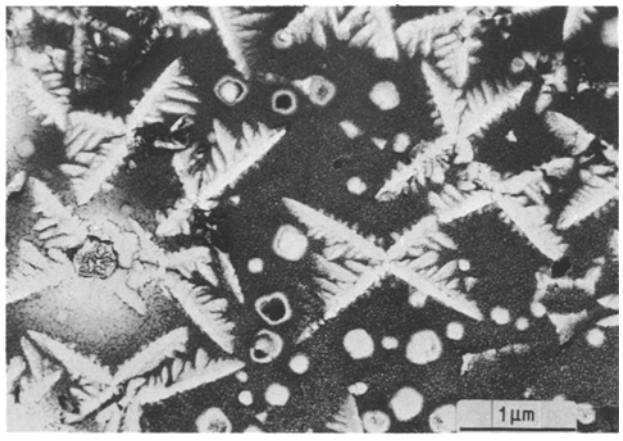

Figure 11 Microstructure of dull side for the $Fe_{80}B_{12}Si_8$ glass annealed at 723 K for 30 min.

$$\alpha = \frac{(n_B^{\alpha} - n_B^{\infty})}{[(n_B^{\alpha} - n_B^{\beta})(n_B^{\infty} - n_B^{\beta})]^{1/2}} \quad (6)$$

where n_B^{α}, n_B^{β}, n_B^{∞}, represent the concentration of boron at the crystal/amorphous interface, in the primary α-iron, and in the amorphous matrix, respectively. Assuming $n_B^{\alpha} = 0.25$ (this concentration is indicated by the eventual crystallization of the matrix into Fe_3B, $n_B^{\beta} = 0.0001$ (see discussion above and [13]). $n_B^{\infty} = 0.12$ (the nominal glass composition), we calculate $\alpha_1 = 0.75$ for one-dimensional growth. Equation 6 can trivially be extended to three-dimensional growth for the simple case of spherical particles as $\alpha_3 = 3^{1/2}\alpha_1 = 1.30$. Using the value for α, and Equation 4, the diffusion coefficient has been estimated versus the temperature for $Fe_{80}B_{12}Si_8$ and is shown in Fig. 15. The pre-exponential factor D_0 as determined from Fig. 14 or 15 is 1.08×10^{-4} m^2 sec^{-1}. The values for Q (see Section 3.3) and D_0 in this alloy are close to the values 1.8 eV, 2×10^{-4} m^2 sec^{-1} reported by Koster in Fe–B binary alloy [12].

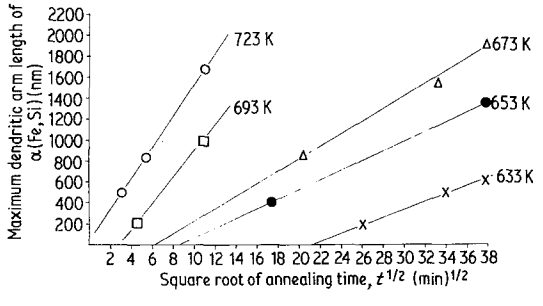

Figure 12 The maximum dendritic arm length of α(Fe, Si) versus the square root of annealing time, for the $Fe_{80}B_{12}Si_8$ glass annealed at five different temperatures, 723, 693, 673, 653 and 633 K.

To compare with the diffusion data for volume diffusion of boron in α-iron, ($Q = 2.7$ eV, $D_0 = 1.0 \times 10^2$ m^2 sec^{-1}) [15], the activation energy (1.6 eV) for boron diffusion in amorphous $Fe_{80}B_{20}Si_8$ is much lower. However, it is close to the activation energy (~ 1.4 to 1.9 eV) for grain-boundary diffusion of boron in α-iron. (The above estimate is based upon the empirical observation that the activation energy for grain-boundary diffusion is generally between 0.5 to 0.7 times that of volume diffusion [16].)

The above analysis, suggests the likelihood of a structure similar to grain boundary in an amorphous metal. Such a structure could be conceptually understood based upon the ideas of Spaeper [17] and is discussed below. Short-range order exists in amorphous metal. The development of a short-range order is considered as a

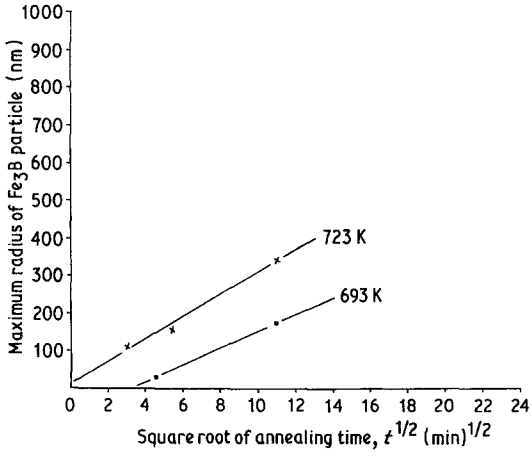

Figure 13 The maximum radius of Fe_3B plotted against the square root of annealing time for the $Fe_{80}B_{12}Si_8$ glass annealed at 723 and 693 K.

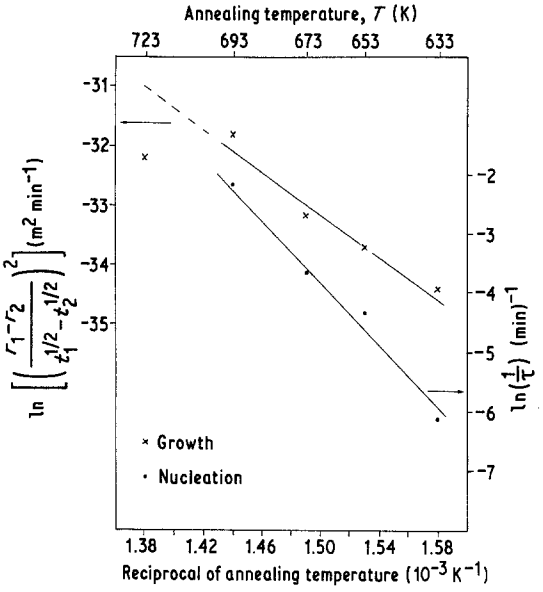

Figure 14 $\ln\{[(r_2-r_1)/(t_2^{1/2}-t_1^{1/2})]^2\}$ plotted against $1/T$ for determining the activation energy for the growth of α(Fe, Si), (left side), and the plot of $\ln(1/\tau)$ against $1/T$ for determining the activation energy for the nucleation of α(Fe, Si).

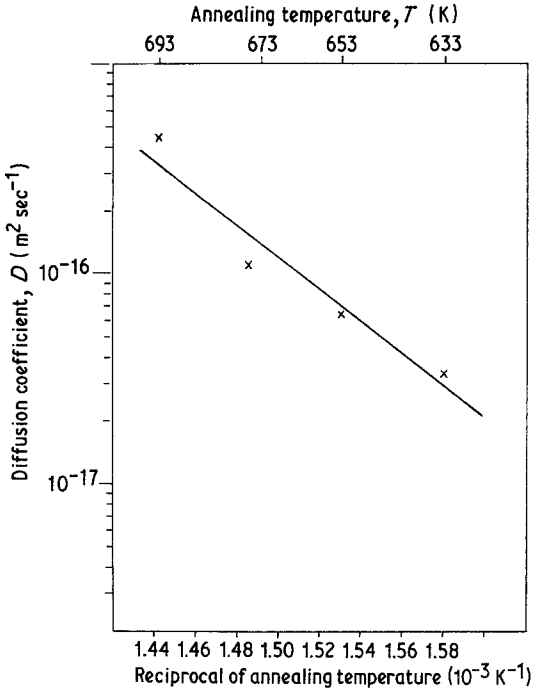

Figure 15 The diffusion coefficient of boron plotted against reciprocal of annealing temperature for the $Fe_{80}B_{12}Si_8$ glass.

process which starts at various points in the specimen and grows as domains with a differing spatial distribution of short range order. A transition zone which is similar to a grain boundary must exist where two domains are adjacent to each other. This zone is likely to be more diffuse than a crystalline grain boundary and can probably be described as a layer in which some of the atoms have "imperfect" short-range order, different from that in either domain. Then, analogous to a grain boundary, this kind of "imperfect" short-range order could provide an easy path for the diffusion of boron in the amorphous matrix, accounting for the low values of Q observed.

4. Conclusions

The crystallization behaviour of the metallic glass alloy $Fe_{80}B_{12}Si_8$ studied by DSC, TEM and XRD shows that the crystallized phases are α(Fe, Si) and Fe_3B in sequence. The activation energy for the nucleation of α(Fe, Si) is 2.3 eV. The α(Fe, Si) has a dendritic shape, and the growth direction of these particles is believed to be the ⟨100⟩ direction. Fe_3B has a cylindrical shape. The distribution of α(Fe, Si) particles is rather uniform in the bulk, but very non-uniform on both surfaces. Significant difference in the microstructure of the two surfaces and composition depth profiles are in agreement with the observation that the nucleation occurs first on the shiny side.

The growth of α(Fe, Si) and Fe_3B obeys a $t^{1/2}$ law and is diffusion controlled. The activation energy for the growth of α(Fe, Si) is 1.6 eV. This lower value may be due to the preferential diffusion of B along a region with "imperfect" short-range order in the metallic glass.

Acknowledgements

We thank Drs L. A. Davis and R. Hasegawa for the support of this project. Helpful discussions with Drs G. Fish and V. R. V. Ramanan are greatly appreciated. Technical assistance provided by G. J. Diercks Jr, J. E. Briggs Jr, and E. A. Musso, is greatly appreciated.

References

1. R. HASEGAWA, G. E. FISH and V. R. V. RAMANAN, in "Proceedings of 4th International Conference on Rapidly Quenched Metals", Sendai, August 1981, edited by T. Masumoto and K. Suzuki (The Japan Institute of Metals, Sendai, 1982) p. 929.
2. A. DATTA, N. J. DeCRISTOFARO and L. A. DAVIS, *ibid.* p. 1007.
3. R. HASEGAWA, V. R. V. RAMANAN and G. E. FISH, *J. Appl. Phys.* **53** (1982) 2276.

4. M. C. NARASIMHAN, US Pat. No. 4 142 571.
5. E. A. MARSEGLIA, *J. Non-Cryst. Mater.* **41** (1980) 31.
6. V. R. V. RAMANAN and G. E. FISH, *J. Appl. Phys.* **53** (1982) 2273.
7. M. AVRAMI, *J. Chem. Phys.* **7** (1939) 1103.
8. J. C. SWARTZ, R. KOSSOWSKY, J. J. HAUGH and R. F. KRAUSE, *J. Appl. Phys.* **52** (1981) 3324.
9. S. RANGANATHAN and M. VON HEIMENDAHL, *J. Mater. Sci.* **16** (1981) 2401.
10. L. A. DAVIS, N. DeCRISTOFARO and C. H. SMITH, in Proceedings of the Conference on Metallic Glasses: Science and Technology, Budapest (1980) p. 1.
11. W. KOSTER and W. HEROLD, in "Glassy Metals I", edited by H. J. Guntherodt and H. Beck (Springer-Verlag, New York, 1981) Ch. 10.
12. W. KOSTER and W. HEROLD, *Scripta Metall.* **12** (1978) 75.
13. M. HANSEN, "Constitution of Binary Alloys", 2nd edn (McGraw-Hill, New York, 1958).
14. C. ZENER, *J. Appl. Phys.* **20** (1949) 950.
15. F. S. BUFFINGTON, K. HIRANO and M. COHEN, *Acta Metall.* **9** (1961) 434.
16. P. G. SHEWMON, "Diffusion in Solids" (McGraw-Hill, New York, 1963).
17. F. SPAEPEN, in "Atomic Scale Structure of Amorphous Solids", edited by G. S. Cargill III and P. Chaudhari (North Holland, New York, 1978) p. 207.

Received 18 August
and accepted 2 September 1982